–Brief Paper–

OPTIMAL MECHANISM DESIGN AND DYNAMIC ANALYSIS OF A 3-LEG 6-DOF LINEAR MOTOR BASED PARALLEL MANIPULATOR

Thong-Shing Hwang and Ming-Yang Liao

ABSTRACT

This paper presents the optimal mechanism design and dynamic analysis of a prototype 3-leg 6-DOF (degree-of-freedom) parallel manipulator. Inverse kinematics, forward kinematics, inverse dynamics and working space characterizing the platform motion are derived. In the presented architecture, the base platform has three linear slideways individually actuated by a synchronous linear servo motor, and each extensible vertical link connecting the upper and base platforms is actuated by an inductive AC servo motor. The linear motors contribute high-speed movements to the upper platform. This kind of architecture using hybrid (linear and AC) motors yields high level performance of motions, especially in the working space. The novel result of maximal working angles is the significant contribution of this architecture. The Taguchi Experimental Method is applied to design the optimal mechanism of the platform system, and the result is used as the actual data to build this system.

KeyWords: 3-leg 6-DOF platform, inverse dynamics, inverse kinematics, taguchi method.

I. INTRODUCTION

The Stewart platform is a six-degree-of-freedom (6-DOF) mechanism with two platforms connected together by six extensible legs. It is an example of a parallel connection robot manipulator. This manipulation structure is obtained through generalization of the mechanism originally proposed by Stewart [1-2] as a flight simulator. There are many research topics concerning this mechanical structure, including its construction, singularity and working space determination, forward and inverse kinematic problem solution, dynamic forces computation, motion control, and practical applications [3-8].

Recently, there has been great interest in the design of spatial multiple-DOF parallel manipulators for specific purposes [9-11]. While many research results concentrating on modeling, analysis and related topics of Stewart platforms have been published in the literature, there has been little research concerning multiple DOF parallel manipulators actuated by hybrid (including linear and AC) motors. Compared to the conventional hydraulic Stewart platforms, the linear motor possesses many advantages, such as direct driving, high level position control accuracy, high speed, fast acceleration, wide bandwidth and ease of control (due to less nonlinearity). The proposed new special architecture, the 3-leg 6-DOF platform system, using hybrid (linear and AC) motors yields high level performance of motions, especially in the working space.

Manuscript received September 9, 2002; revised April 2, 2003; accepted May 1, 2003

The authors are with Institute of Automatic Control Engineering, Feng Chia University, Taichung 40724, Taiwan, R.O.C.

II. PLATFORM SYSTEM DESIGN

2.1 New architecture

The new architecture, as shown in Fig. 1, is constructed using three extensible legs sliding on three linear slideways, each actuated by a synchronous linear servo motor. The extensible legs are actuated by inductive AC servo motors. The top views of the upper and base platforms are shown in Fig. 2.

2.2 Degree of freedom analysis

Intuitively, the degree-of-freedom value of a mechanism is equal to the degrees of freedom associated

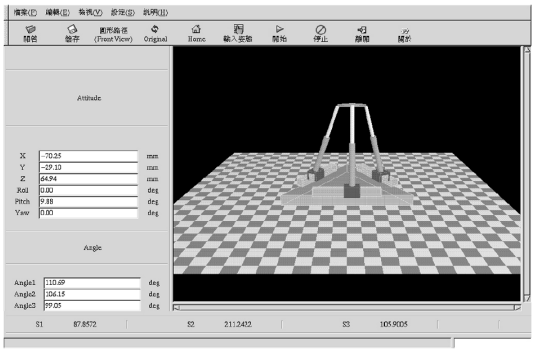

Fig. 1. 3D graphical illustration of the hybrid motor driven platform.

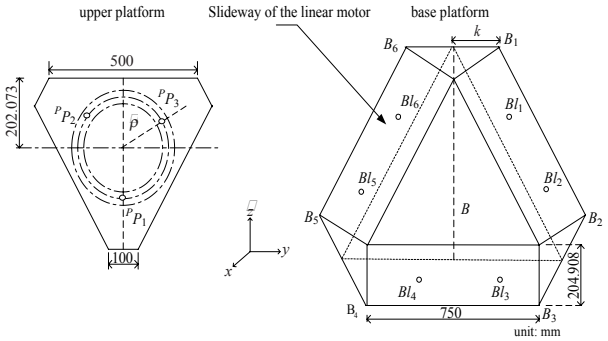

Fig. 2. Top view of the upper and base platforms.

with all the moving links minus the number of constraints imposed by the joints. Hence, if the links are all free of constraints, then the degrees of freedom of an n-link mechanism, with one of its links fixed to the ground, will be equal to $d(n-1)$. However, the total number of constraints imposed by the joints is equal to ΣC_i. Hence the degree-of-freedom value of a mechanism is generally given by $M = d(n-1) - \Sigma c_i$, where $d = 6$ for spatial mechanisms; n is the number of links in a mechanism, including the fixed link. Due to $d = c_i + f_i$, where f_i represents the degrees of relative motion permitted by joint i,

$$\sum_{i=1}^{g} c_i = \sum_{i=1}^{g} (d - f_i) = dg - \sum_{i=1}^{g} f_i,$$

where g is the number of joints in a mechanism. Therefore, the degree-of-freedom value of a mechanism is

$$M = d(n-g-1) + \sum_{i=1}^{g} f_i. \tag{1}$$

For example, the degree-of-freedom value of the 3-leg 6-DOF parallel manipulator can be calculated as follows:

$$n = 3x3 + 2 = 11, g = 4x3 = 12,$$

$$\sum_{i=1}^{g} f_i = 3\times 3 + (1\times 3)\times 3 = 18,$$

$$M = 6(11-12-1) + 18 = 6.$$

Note that the position and orientation of the moving platform are controlled by the lengths of the three legs actuated by three 1-DOF prismatic joints. Since each leg is itself orthogonal to a linear slideway, not only does it rotate about the linear slideway, but it also slides on the linear slideway, so each leg is connected to the base through a 1-DOF revolute joint and a 1-DOF prismatic joint, and connected to the moving platform by a 3-DOF spherical joint.

III. KINEMATICS ANALYSIS

3.1 Coordinate transformation

In Fig. 2, ${}^{P}\boldsymbol{P_i}$ (i = 1, 2, 3) denote the position vectors of the joint points between the three links and the moving platform. These are concentric joint points with respect to the upper platform coordinate frame $\{P\}$. $\boldsymbol{B}_i$ (i = 1, 2, 3) denote the position vectors of the joint points on the base platform with respect to the base platform coordinate frame $\{B\}$. The mechanism has been designed as a vehicle driving simulator which possesses quick pitching, yawing and rolling motions.

Assume that the coordinate systems $\{B\}$ and $\{P\}$, with their origins at the platform's mass center, are related to the base platform and the moving platform, respectively. We define the Cartesian coordinate vector $[x \;\; y \;\; z \;\; \phi \;\; \theta \;\; \psi]^T$, where $[x \;\; y \;\; z]^T$ and $[\phi \;\; \theta \;\; \psi]^T$ denote, respectively, the position and orientation of the moving platform's mass center. We also define the joint coordinate vector $[l_1 \;\; l_2 \;\; l_3 \;\; d_1 \;\; d_2 \;\; d_3]^T$, where d_i, i = 1, 2, 3, is the distance between the ith joint and the starting position of the slideway on the base platform, and l_i, i = 1, 2, 3, is the length of the vertical link.

We can develop kinematic relations of positions with respect to the base frame and platform frame. The orientation representation gives the following Euler orientation matrix, which provides a coordinate transformation from frame $\{P\}$ to frame $\{B\}$:

$$\boldsymbol{R} = \begin{bmatrix} c\psi c\theta & c\psi s\theta s\phi - s\psi c\phi & c\psi s\theta c\phi + s\psi s\phi \\ s\psi c\theta & s\psi s\theta s\phi + c\psi c\phi & s\psi s\theta c\phi - c\psi s\phi \\ -s\theta & c\theta s\phi & c\theta c\phi \end{bmatrix}. \tag{2}$$

3.2 Inverse kinematics

The purpose of inverse kinematics analysis is to determine the corresponding joint coordinate vector $[l_1 \;\; l_2 \;\; l_3 \;\; d_1 \;\; d_2 \;\; d_3]^T$ on the base platform under the given Cartesian coordinate vector $[x \;\; y \;\; z \;\; \phi \;\; \theta \;\; \psi]^T$ of the upper platform's mass center.

Referring to Fig. 2, the coordinates of the joints ${}^{P}\boldsymbol{P_i}$,

i =1, 2, 3 on the moving platform are given in the following:

$$^{P}P_1 = (\frac{2}{3}\rho, 0, 0), ^{P}P_2 = (-\frac{1}{3}\rho, -\frac{\rho}{\sqrt{3}}, 0),$$
$$^{P}P_3 = (-\frac{1}{3}\rho, \frac{\rho}{\sqrt{3},}, 0),$$

where ρ is the height of the equilateral triangular forming the moving plate. For the base platform, the coordinates of the hexagon terminal points shown in Fig. 2 are given as follows:

$$BB_1 = (\frac{-2}{3}B, k, 0),\ BB_2 = (\frac{B}{3} - k_1, \frac{2}{3}B\cos\frac{\pi}{6} + k_2, 0),$$
$$BB_3 = (\frac{B}{3} - k_1, \frac{2}{3}B\cos\frac{\pi}{6} - k_2, 0),$$
$$BB_4 = (\frac{B}{3} + k_1, -\frac{2}{3}B\cos\frac{\pi}{6} + k_2, 0),$$
$$BB_5 = (\frac{B}{3} - k_1, -\frac{2}{3}B\cos\frac{\pi}{6} - k_2, 0),\ BB_6 = (-\frac{2}{3}B, k, 0),$$

where B is the height of the equilateral triangular formed within the base plate, κ is the half length from BB_6 to BB_1, $k_1 = k\sin(\pi/6)$, and $k_2 = k\cos(\pi/6)$.

Here, we consider the vector diagram for the ith link shown in Fig. 3. It is convenient to treat the links as lines and represent them as line coordinates. From Fig. 3, the line vector of the ith link from $\boldsymbol{B_i}$ to $\boldsymbol{P_i}$ with respect to frame $\{B\}$ can be expressed as follows:

$$\boldsymbol{L_i} = \boldsymbol{T_v} + \boldsymbol{R}\,^{p}\boldsymbol{P_i} - \boldsymbol{B_i}, \quad i = 1, 2, 3, \tag{3}$$

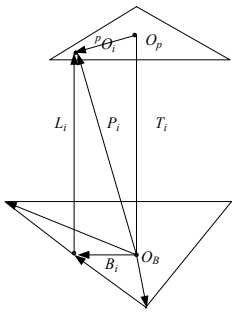

Fig.3. Position and orientation of the upper platform.

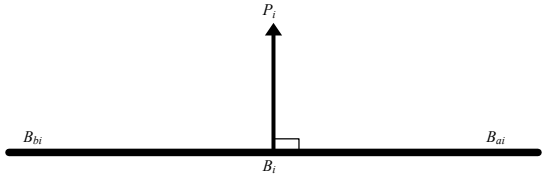

Fig. 4. Coordinate relation diagram between the horizontal link and the vertical link.

where $\boldsymbol{T_v}$ denotes the origin's line vector of frame $\{P\}$ with respect to frame $\{B\}$.

From Fig. 4, we have

$$B_{iy} = \frac{B_{biy} - B_{aiy}}{B_{bix} - B_{aix}} B_{ix} + \frac{B_{bix}B_{aiy} - B_{biy}B_{aix}}{B_{bix} - B_{aix}},\ i = 1, 2, 3, \tag{4}$$

where $B_{ai} = [B_{aix} \quad B_{aiy} \quad 0]^T$ and $B_{bi} = [B_{bix} \quad B_{biy} \quad 0]^T$ indicate, respectively, the starting and terminal position vectors of the ith linear motor's translator. Furthermore, since the vertical link is orthogonal to the horizontal link as shown in Fig. 4, we have the following constraints:

$$(B_{bi} - B_{ai}) \cdot L_i = 0,\ i = 1, 2, 3. \tag{5}$$

Combining (5) and (6), B_{ix} can be solved for all motor translators:

$$B_{ix} = \frac{(B_{bix} - B_{aix})P_{ix} + (P_{iy} - C)(B_{biy} - B_{aiy})}{(B_{bix} - B_{aix}) + A(B_{biy} - B_{aiy})}, \tag{6}$$

where $A = \dfrac{(B_{biy} - B_{aiy})}{(B_{bix} - B_{aix})}$, $C = \dfrac{B_{bix}B_{aiy} - B_{biy}B_{aix}}{B_{bix} - B_{aix}}$. Equation (7) ensures that all B_{ix} are within the slideway of the linear motor. In the same way, B_{iy} can also be determined.

Next, we turn our attention to the link frames $\{\boldsymbol{i_i}, \boldsymbol{j_i}, \boldsymbol{k_i}\}$, i =1, 2, 3. The unit vector $\boldsymbol{i_i}$ of the link coordinate ^{i}XYZ is defined as follows:

$$\boldsymbol{i_i} = \frac{\boldsymbol{L_i}}{\|\boldsymbol{L_i}\|} = i_{ix}\,\boldsymbol{i} + i_{iy}\,\boldsymbol{j} + i_{iz}\,\boldsymbol{k}, \tag{7}$$

$$\boldsymbol{j_i} = \frac{\boldsymbol{i_i} \times (-\boldsymbol{k})}{\|\boldsymbol{i_i} \times (-\boldsymbol{k})\|} = j_{ix}\,\boldsymbol{i} + j_{iy}\,\boldsymbol{j} + j_{iz}\,\boldsymbol{k}, \tag{8}$$

$$\boldsymbol{k_i} = \boldsymbol{i_i} \times \boldsymbol{j_i} = k_{ix}\,\boldsymbol{i} + k_{iy}\,\boldsymbol{j} + k_{iz}\,\boldsymbol{k}. \tag{9}$$

This gives a coordinate transformation matrix from frame $\{i\}$ to frame $\{B\}$ as follows:

$$\boldsymbol{R_i} = \begin{bmatrix} i_{ix} & i_{iy} & i_{iz} \\ j_{ix} & j_{iy} & j_{iz} \\ k_{ix} & k_{iy} & k_{iz} \end{bmatrix}, \quad i = 1, 2, 3 \tag{10}$$

The coordinate transformation matrix from frame $\{B\}$ to frame $\{i\}$ is the transpose of $\boldsymbol{R_i}(\boldsymbol{R_i^T})$.

The angular rates of the links can be derived from the motion description of the relative orientation of frame $\{i\}$ with the respect to frame $\{B\}$. We first rotate frame $\{B\}$ about the Z-axis by an angle ϕ_i to get frame $\{B'\}$, then rotate $\{B'\}$ about the Y'-axis by an angle θ_i to get frame $\{B''\}$, and finally rotate $\{B''\}$ about the Z''-axis

by an angle ψ_i to get frame $\{i\}$. This sequence gives a transformation matrix as follows:

$$\boldsymbol{R}_i^T = \begin{bmatrix} c\phi_i c\theta_i c\psi_i - s\phi_i s\psi_i & -c\phi_i c\theta_i s\psi_i - s\phi_i c\psi_i & c\phi_i s\theta_i \\ s\phi_i c\theta_i c\psi_i + c\phi_i s\psi_i & -s\phi_i c\theta_i s\psi_i + c\phi_i c\psi_i & s\phi_i s\theta_i \\ -s\theta_i c\psi_i & s\theta_i s\psi_i & c\theta_i \end{bmatrix}. \tag{11}$$

Combining (12) and (13), the corresponding Euler angles of the ith link can be obtained:

$$\begin{aligned} &\phi_i = \tan^{-1}(\frac{k_{iy}}{k_{ix}}), \theta_i = \tan^{-1}(\frac{k_{ix}\cos\phi_i + k_{iy}\sin\phi_i}{k_{iz}}), \\ &\psi_i = \tan^{-1}(\frac{-i_{ix}\sin\phi_i + i_{iy}\cos\phi_i}{-j_{ix}\sin\phi_i + j_{iy}\cos\phi_i}). \end{aligned} \tag{12}$$

In this particular architecture, since the vertical link is orthogonal to the horizontal link, only the angle θ_i needs to be determined; the angular velocity ω_i and angular acceleration can be expressed as follows:

$$\omega_i = \dot{\theta}_i, a_i = \ddot{\theta}_i.$$

Similarly, to find the angular velocity of the moving platform, we first rotate frame $\{B\}$ about the Z-axis by an angle ψ_p, then rotate about the Y'-axis by an angle θ_p, and finally rotate about the X''-axis by an angle ϕ_p. The angular velocity ω_p can then be represented as follow:

$$\begin{aligned} \omega_p &= \begin{bmatrix} \omega_{px} & \omega_{py} & \omega_{pz} \end{bmatrix}^T \\ &= \dot{\psi}_p\, \boldsymbol{k} + \dot{\theta}_p\, \boldsymbol{j}' + \dot{\phi}_p\, \boldsymbol{k}'' = \begin{bmatrix} -\dot{\psi}_p s\theta_p + \dot{\phi}_p \\ \dot{\psi}_p c\theta_p s\phi_p + \dot{\theta}_p c\phi_p \\ \dot{\psi}_p c\theta_p c\phi_p - \dot{\theta}_p s\phi_p \end{bmatrix}, \end{aligned} \tag{13}$$

and the angular acceleration $\boldsymbol{a_p}$ also can be obtained by differentiating $\boldsymbol{\omega_p}$ directly.

3.3 Forward kinematics

The forward kinematics are used to calculate the position and attitude of the moving platform for the given $\boldsymbol{B_i}$ and l_i. The forward kinematics problem requires solving for the solution from a series of non-linear equations, and this usually leads to multiple solutions. In order to quickly obtain a reliable solution to the forward kinematics problem, the Newton-Difference numerical method is adopted. Using the constraint equations of the links, we have

$$\Phi_{i1} = (P_i - B_i)^T (P_i - B_i) - l_i^2 = 0, \quad i = 1,2,3, \tag{14}$$

$$\Phi_{i2} = (P_k - B_k)^T \cdot d_k = 0, \ i = 4,5,6, \ k = i-3, \tag{15}$$

where d_k is the unit vector of the sliding-way for the linear motor, $l_i = |\boldsymbol{L}_i|$.

Differentiating (14) and (15) with respect to time t gives

$$\begin{aligned} &\frac{\partial \Phi}{\partial t} = \Phi_x \dot{X} + \Phi_q \dot{q} = 0, \\ &\Phi = \begin{bmatrix} \Phi_{11} & \Phi_{21} & \Phi_{31} & \Phi_{42} & \Phi_{52} & \Phi_{62} \end{bmatrix}, \end{aligned} \tag{16}$$

where $\dot{\boldsymbol{X}} = [\dot{p} \ \ \dot{\vartheta}] = [\dot{p} \ \ \omega_p]^T = [\dot{x} \ \ \dot{y} \ \ \dot{z} \ \ \omega_{px} \ \ \omega_{py} \ \ \omega_{pz}]^T$,

$$\dot{q} = \begin{bmatrix} \dot{d}_1 & \dot{d}_2 & \dot{d}_3 & \dot{l}_1 & \dot{l}_2 & \dot{l}_3 \end{bmatrix}^T,$$

using

$$\frac{\partial \Phi_{i1}}{\partial \boldsymbol{p}} \dot{\boldsymbol{p}} = 2(\boldsymbol{T}_v + \boldsymbol{m}_i - \boldsymbol{B}_i)^T \dot{\boldsymbol{p}} = 2\boldsymbol{L}_i^T \dot{\boldsymbol{p}}, \ i = 1,2,3, \tag{17}$$

$$\begin{aligned} &\frac{\partial \Phi_{i2}}{\partial \boldsymbol{p}} \dot{\boldsymbol{p}} = \frac{(\boldsymbol{T}_v + \boldsymbol{m}_k - \boldsymbol{B}_k)^T \cdot \boldsymbol{d}_k}{\partial \boldsymbol{p}} \dot{\boldsymbol{p}} = \boldsymbol{d}_k^T \dot{\boldsymbol{p}}, \\ &i = 4,5,6, \ k = i-3, \end{aligned} \tag{18}$$

$$\begin{aligned} \frac{\partial \Phi_{i1}}{\partial \boldsymbol{\vartheta}} \boldsymbol{\omega_p} &= 2(\dot{\boldsymbol{R}}^p \boldsymbol{P}_i)^T \boldsymbol{L}_i = 2(\omega_p \times \boldsymbol{R}^P \boldsymbol{P}_i)^T \boldsymbol{L}_i \\ &= 2(\boldsymbol{m}_i \times \boldsymbol{L}_i)^T \omega_p, \quad i = 1,2,3, \end{aligned} \tag{19}$$

$$\begin{aligned} \frac{\partial \Phi_{i2}}{\partial \boldsymbol{\vartheta}} \boldsymbol{\omega}_p &= \frac{\partial (\boldsymbol{T}_v + \boldsymbol{R}^P \boldsymbol{P}_k - \boldsymbol{B}_k)^T \boldsymbol{d}_k}{\partial \vartheta} \boldsymbol{\omega}_p = (\dot{\boldsymbol{R}}^P \boldsymbol{P}_k)^T \boldsymbol{d}_k \\ &= (\boldsymbol{m}_i \times \boldsymbol{d}_k)^T \boldsymbol{\omega}_p, \quad i = 4,5,6, \quad k = i-3, \end{aligned} \tag{20}$$

where $\boldsymbol{m_i} = \boldsymbol{R^P P_i}$, $\boldsymbol{L_i} = \boldsymbol{T_v} + \boldsymbol{m_i} - \boldsymbol{B_i}$, and $\boldsymbol{\omega_p}$ is the angular rate of the platform. $\boldsymbol{\Phi}_x$ can be expressed as

$$\boldsymbol{\Phi}_x = \begin{bmatrix} \{2(\boldsymbol{T_v} + \boldsymbol{m}_1 - \boldsymbol{B}_1)\}^T & \{2\boldsymbol{m}_1 \times (\boldsymbol{T_v} + \boldsymbol{m}_1 - \boldsymbol{B}_1)\}^T \\ \{2(\boldsymbol{T_v} + \boldsymbol{m}_2 - \boldsymbol{B}_2)\}^T & \{2\boldsymbol{m}_2 \times (\boldsymbol{T_v} + \boldsymbol{m}_2 - \boldsymbol{B}_2)\}^T \\ \{2(\boldsymbol{T_v} + \boldsymbol{m}_3 - \boldsymbol{B}_3)\}^T & \{2\boldsymbol{m}_3 \times (\boldsymbol{T_v} + \boldsymbol{m}_3 - \boldsymbol{B}_3)\}^T \\ \boldsymbol{d}_1^T & (\boldsymbol{m}_1 \times \boldsymbol{d}_1)^T \\ \boldsymbol{d}_2^T & (\boldsymbol{m}_2 \times \boldsymbol{d}_2)^T \\ \boldsymbol{d}_3^T & (\boldsymbol{m}_3 \times \boldsymbol{d}_3)^T \end{bmatrix}. \tag{21}$$

Equations (14) and (15) can be expanded as follows:

$$\Phi(X) + \frac{\partial \Phi}{\partial X} \Delta X + \cdots = 0. \tag{22}$$

Ignoring the high-order terms, the above equation can be expressed as follows:

$$\Delta X = -(\Phi_x^{-1} \Phi) \tag{23}$$

with Φ_X defined by (21). The Newton-Difference numerical method can then be used to solve for $\boldsymbol{X}$ with respect to this equation.

IV. DYNAMICS ANALYSIS

The purpose of inverse dynamics analysis is to determine the required thrust forces of the linear motor and the AC servo motor for a given motion trajectory of the moving platform. We analyze the system dynamics of the moving platform and links using the Newton-Euler equations of motion, which can be formulated by considering the free-body diagrams of the links and moving platform separately.

4.1 Link dynamics

Let us focus on the i th link's mass center $\boldsymbol{O_i}$ as shown in Fig. 5. Each link is placed along the X_i axis; therefore, its inertia tensor about X_i, Y_i and Z_i is a diagonal matrix with diagonal elements I_{ixx}, I_{iyy} and I_{izz}. The angular momentum of the ith link is

$$\boldsymbol{H_i} = I_{ixx}\omega_{ix}\ \boldsymbol{i_i} + I_{iyy}\omega_{iy}\ \boldsymbol{j_j} + I_{izz}\omega_{iz}\ \boldsymbol{k_i}. \tag{24}$$

The rate of change of $\boldsymbol{H_i}$ is given by

$$\dot{\boldsymbol{H}}_{\boldsymbol{i}} = (\dot{\boldsymbol{H}}_{\boldsymbol{i}})_{\boldsymbol{xyzi}} + \boldsymbol{\omega_i} \times \boldsymbol{H_i}. \tag{25}$$

It follows from Fig. 5 that the torque about the link's mass center $\boldsymbol{O_i}$ is given by

$$\sum \boldsymbol{M_{O_i}} = {}^{\boldsymbol{i}}\boldsymbol{r_{pi}} \times {}^{\boldsymbol{i}}\boldsymbol{F_{pi}} + {}^{\boldsymbol{i}}\boldsymbol{r_{bi}} \times {}^{\boldsymbol{i}}\boldsymbol{F_{bi}}, \tag{26}$$

where ${}^{\boldsymbol{i}}\boldsymbol{r_{pi}}$ is the vector from $\boldsymbol{O_i}$ to $\boldsymbol{P_i}$ with respect to link frame $\{i\}$, and ${}^{\boldsymbol{i}}\boldsymbol{r_{bi}}$ is the vector from $\boldsymbol{O_i}$ to $\boldsymbol{B_i}$ with respect to frame $\{i\}$.

The equations of rotational motion of the ith link can be obtained by equating the rate of change of $\boldsymbol{H_i}$ with the external moment. Equating (25) and (26), the relations between ${}^iF_{pix}$, ${}^iF_{piy}$, ${}^iF_{piz}$ and ${}^iF_{bix}$, ${}^iF_{biy}$, ${}^iF_{biz}$ can be described by

$$\begin{aligned}&(I_{izz}\omega_{iz}\omega_{iy} - I_{iyy}\omega_{iy}\omega_{iz}) + \dot{I}_{ixx}\omega_{ix} + I_{ixx}\dot{\omega}_{ix}\\ &= ({}^i r_{piy}\,{}^i F_{piz} - {}^i r_{piz}\,{}^i F_{piy}) + ({}^i r_{biy}\,{}^i F_{biz} - {}^i r_{biz}\,{}^i F_{biy}),\end{aligned} \tag{27}$$

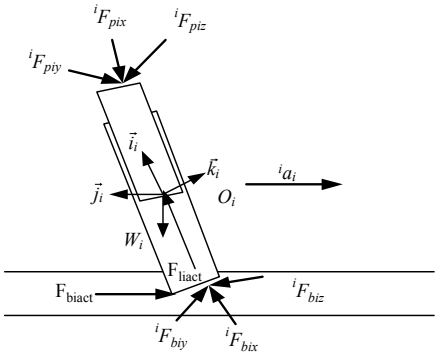

Fig. 5. Free-body diagram of forces on the linear motor and link.

$$\begin{aligned}&-(I_{izz}\omega_{iz}\omega_{ix} - I_{ixx}\omega_{ix}\omega_{iz}) + \dot{I}_{iyy}\omega_{iy} + I_{iyy}\dot{\omega}_{iy}\\ &= -({}^i r_{pix}\,{}^i F_{piz} - {}^i r_{piz}\,{}^i F_{pix}) - ({}^i r_{bix}\,{}^i F_{biz} - {}^i r_{biz}\,{}^i F_{bix}),\end{aligned} \tag{28}$$

$$\begin{aligned}&(I_{iyy}\omega_{iy}\omega_{ix} - I_{ixx}\omega_{ix}\omega_{iy}) + \dot{I}_{izz}\omega_{iz} + I_{iz}\dot{\omega}_{iz}\\ &= ({}^i r_{pix}\,{}^i F_{piy} - {}^i r_{piy}\,{}^i F_{pix}) + ({}^i r_{bix}\,{}^i F_{biy} - {}^i r_{biy}\,{}^i F_{bix}).\end{aligned} \tag{29}$$

Since $\dot{I}_{ixx} = \dot{I}_{iyy} = \dot{I}_{izz} = 0$, ${}^iF_{pix}$ and ${}^iF_{bix}$ passing through the link's mass center do not generate torques, and ${}^{\boldsymbol{i}}\boldsymbol{r_{pi}}$ and ${}^{\boldsymbol{i}}\boldsymbol{r_{bi}}$ only have values on the X_i-axis. Also, the vertical link is orthogonal to the slideway, which means that only momentum exists about the Y-axis relative to frame{i}. Therefore, the above equations can be simplified to only one constraint equation:

$${}^i r_{pix}\,{}^i F_{piz} + {}^i r_{bix}\,{}^i F_{biz} = I_{izz}\omega_{iz}\omega_{ix} - I_{ixx}\omega_{ix}\omega_{iz} - I_{iyy}\dot{\omega}_{iy} \tag{30}$$

We now proceed to find the total force acting on the link's mass center. From the free-body diagrams shown in Fig. 5 and Fig. 6, we have

$${}^{\boldsymbol{i}}\boldsymbol{F_{bi}} - {}^{\boldsymbol{i}}\boldsymbol{F_{pi}} - \boldsymbol{R_i^T W_{li}} = m_{li}\,{}^{\boldsymbol{i}}\ddot{\boldsymbol{r}}_{\boldsymbol{ic.m}}, \tag{31}$$

where $\boldsymbol{W}_{li} = [0 \quad 0 \quad W_{liz}]^T$ with W_{liz} and m_{li} being, respectively, the weight and mass of the ith link, and the acceleration at the link's mass center is given by

$$\begin{aligned}{}^{\boldsymbol{i}}\ddot{\boldsymbol{r}}_{\boldsymbol{ic.m}} &= \boldsymbol{R_i^T}\ddot{\boldsymbol{r}}_{\boldsymbol{Bi}} + {}^{\boldsymbol{i}}\ddot{\boldsymbol{r}}_{\boldsymbol{Bic}}\\ &= \boldsymbol{R_i^T}\ddot{\boldsymbol{r}}_{\boldsymbol{Bi}} + \boldsymbol{a_i} \times {}^{\boldsymbol{i}}\boldsymbol{r_{Bic}} + \boldsymbol{\omega_i} \times (\boldsymbol{\omega_i} \times {}^{\boldsymbol{i}}\boldsymbol{r_{Bic}}).\end{aligned} \tag{32}$$

Based on this expression, we have

$${}^iF_{bix} = m_{li}\,{}^i\ddot{r}_{ic.mx} - s\theta c\psi W_{liz} + {}^iF_{pix}, \tag{33}$$

$${}^iF_{biy} = m_{li}\,{}^i\ddot{r}_{ic.my} + s\theta c\psi W_{liz} + {}^iF_{piy}, \tag{34}$$

$${}^iF_{biz} = m_{li}\,{}^i\ddot{r}_{ic.mz} + c\theta W_{liz} + {}^iF_{piz}. \tag{35}$$

Substituting (35) into (30) yields

$${}^iF_{piz} = \begin{bmatrix} I_{izz}\mathrm{W}_{iz}\mathrm{W}_{ix} - I_{ixx}\mathrm{W}_{ix}\mathrm{W}_{iz} - I_{iyy}\dot{\mathrm{W}}_{iy} \\ -{}^i r_{bix} m_i\,{}^i\ddot{r}_{ic.mz} - {}^i r_{bix}(c\theta_i) W_{liz} \end{bmatrix} / ({}^i r_{pix} + {}^i r_{bix}), \tag{36}$$

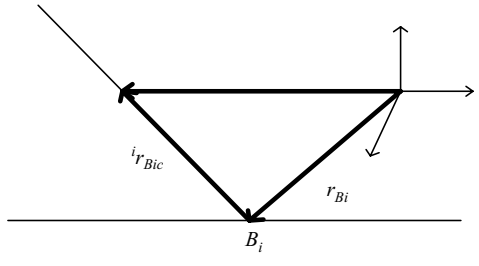

Fig. 6. Relation between the link and the sliding joint of the linear motor.

where ${}^{i}r_{pix}$ and ${}^{i}r_{bix}$ have the same length as ${}^{i}r_{Bicx}$. Substituting ${}^{i}F_{piz}$ from (36) into (35), we can get ${}^{i}F_{biz}$.

4.2 Moving platform dynamics

Only the force terms ${}^{i}F_{piz}$ and ${}^{i}F_{biz}$ have been obtained in the equations of link motion. To calculate the force terms ${}^{i}F_{pix}$ and ${}^{i}F_{piy}$, the moving platform dynamics should be taken into consideration.

The angular momentum of the upper platform is described by

$$\boldsymbol{H_p} = I_{pxx}\omega_{px}\boldsymbol{i_p} + I_{pyy}\omega_{py}\boldsymbol{j_p} + I_{pzz}\omega_{pz}\boldsymbol{k_p}, \tag{37}$$

where I_{pxx}, I_{pyy} and I_{pzz} are, respectively, the mass moments of inertia of the upper platform about the X, Y and Z axes of frame $\{P\}$. The corresponding angular momentum change is

$$\dot{\boldsymbol{H}}_{\boldsymbol{p}} = (\dot{\boldsymbol{H}}_{\boldsymbol{p}})_{\boldsymbol{xyzp}} + \boldsymbol{\omega_p} \times \boldsymbol{H_p}. \tag{38}$$

The total torque acting on the upper platform mass center $\boldsymbol{O_p}$ is given by

$$\sum \boldsymbol{M}_{\boldsymbol{O_F}} = \sum_{\boldsymbol{i}=1}^{3} {}^{\boldsymbol{p}}\boldsymbol{P_i} \times {}^{\boldsymbol{p}}\boldsymbol{P_{pi}}, \tag{39}$$

where ${}^{\boldsymbol{P}}\boldsymbol{F_{pi}} = \boldsymbol{R^T R_i}{}^{i}\boldsymbol{F_{pi}} = \boldsymbol{R_{pi}}{}^{i}\boldsymbol{F_{pi}}$, ${}^{\boldsymbol{P}}\boldsymbol{F_{pi}}$ can be expressed on coordinate frame $\{i\}$ by the rotation matrix $\boldsymbol{R_{pi}} = \boldsymbol{R^T R_i}$. Referring to Fig. 7, the angular momentum change of the upper platform is equal to the torque acting on $\boldsymbol{O_p}$. Through some manipulations, we have

$$\begin{aligned}
&\sum_{i=1}^{3} {}^{p}P_{iy}(R_{pi31}{}^{i}F_{pix} + R_{pi32}{}^{i}F_{piy} + R_{pi33}{}^{i}F_{piz}) \\
&= I_{pxx}\dot{\omega}_{px} + (I_{pzz} - I_{pyy})\omega_{py}\omega_{pz}, \\
&-\sum_{i=1}^{3} {}^{p}P_{ix}(R_{pi31}{}^{i}F_{pix} + R_{pi32}{}^{i}F_{piy} + R_{pi33}{}^{i}F_{piz}) \\
&= I_{pyy}\dot{\omega}_{py} + (I_{pxx} - I_{pzz})\omega_{px}\omega_{pz}, \\
&\sum_{i=1}^{3}\Big[{}^{p}P_{ix}(R_{pi21}{}^{i}F_{pix} + R_{pi22}{}^{i}F_{piy} + R_{pi23}{}^{i}F_{piz}) \\
&- {}^{p}P_{iy}(R_{pi11}{}^{i}F_{pix} + R_{pi12}{}^{i}F_{piy} + R_{pi13}{}^{i}F_{piz})\Big] \\
&= I_{pzz}\dot{\omega}_{pz} + (I_{pyy} - I_{pxx})\omega_{py}\omega_{px}.
\end{aligned} \tag{40}$$

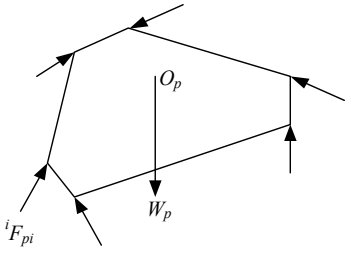

Fig. 7. Forces acting on the upper platform.

By itself, (40) is not sufficient to solve for the required force ${}^{i}F_{pix}$. We need to combine the following auxiliary force and torque equations to determine this term. From Fig. 7, we have the force equation on $\boldsymbol{O_p}$:

$$-\boldsymbol{W_p} + \sum_{\boldsymbol{i}=1}^{3} \boldsymbol{R_i}\,{}^{\boldsymbol{i}}\boldsymbol{F_{pi}} = \boldsymbol{m_p a_p}, \tag{41}$$

where $\boldsymbol{W_p} = [0 \quad 0 \quad W_p]^T$ with W_p and m_p being, respectively, the weight and mass of the upper platform; $\boldsymbol{a_p}$ denotes the acceleration of the upper platform. Expanding $\boldsymbol{R_i^i F_{pi}}$, (41) can be expressed as

$$\begin{aligned}
&\sum_{i=1}^{3}(R_{i11}{}^{i}F_{pix} + R_{i12}{}^{i}F_{piy} + R_{i13}{}^{i}F_{piz}) = m_p a_{px}, \\
&\sum_{i=1}^{3}(R_{i21}{}^{i}F_{pix} + R_{i22}{}^{i}F_{piy} + R_{i23}{}^{i}F_{piz}) = m_p a_{py}, \\
&\sum_{i=1}^{3}(R_{i31}{}^{i}F_{pix} + R_{i32}{}^{i}F_{piy} + R_{i33}{}^{i}F_{piz}) - W_p = m_p a_{pz}.
\end{aligned} \tag{42}$$

Referring to (40) and (42), a compact representation of these six linear equations can be expressed as

$$[D]\begin{bmatrix} {}^{i}F_{px} \\ {}^{i}F_{py} \end{bmatrix} = [Q], \tag{43}$$

where:

$$\begin{aligned}
{}^{\boldsymbol{i}}\boldsymbol{F_{px}} &= \begin{bmatrix} {}^{\boldsymbol{i}}\boldsymbol{F_{p1x}} & {}^{\boldsymbol{i}}\boldsymbol{F_{p2x}} & {}^{\boldsymbol{i}}\boldsymbol{F_{p3x}} \end{bmatrix}, \\
{}^{\boldsymbol{i}}\boldsymbol{F_{py}} &= \begin{bmatrix} {}^{\boldsymbol{i}}\boldsymbol{F_{p1y}} & {}^{\boldsymbol{i}}\boldsymbol{F_{p2y}} & {}^{\boldsymbol{i}}\boldsymbol{F_{p3y}} \end{bmatrix}
\end{aligned}$$

Now that ${}^{i}F_{pix}$ and ${}^{i}F_{piy}$ have been solved, we can proceed to find ${}^{i}F_{bix}$ and ${}^{i}F_{biy}$ from (27) and (28).

As the forces ${}^{i}F_{pix}$, ${}^{i}F_{piy}$, ${}^{i}F_{piz}$, ${}^{i}F_{bix}$, ${}^{i}F_{biy}$ and ${}^{i}F_{biz}$ acting on the ith link have been determined, the actuating force F_{biact} of the linear motor can be determined by projecting ${}^{\boldsymbol{i}}\boldsymbol{F_{bi}}$ into the slideway of the linear motor, i.e:

$$F_{biact} = \left\| \boldsymbol{R_i}\,{}^{\boldsymbol{i}}\boldsymbol{F_{bi}} \right\| \cos\theta_i, \tag{44}$$

where $\cos\theta_i = \boldsymbol{u_{bi}^T R_i}\,{}^{\boldsymbol{i}}\boldsymbol{F_{bi}} / \left\| \boldsymbol{R_i}\,{}^{\boldsymbol{i}}\boldsymbol{F_{bi}} \right\|$, $\boldsymbol{u_{bi}}$ is the unit direction vector of the slideway. Based on this equation, we can calculate the actuating force on each linear motor from the above inverse dynamic analysis of the platform system. The magnitude of the required actuating force for each motor is given by F_{biact}.

Meanwhile, we can calculate the actuating force on each flexible vertical leg using the following force equation for the moving vertical leg:

$${}^{i}F_{liact} = {}^{i}F_{pix} + R_i^T\,{}^{i}W_{\ell ix} + m_{li}\,{}^{i}\ddot{r}_{bic}. \tag{45}$$

V. OPTIMAL MECHANISM DESIGN OF THE PLATFORM SYSTEM

The optimal mechanism design of the platform was constructed as a 3-leg 6-DOF system by using the Taguchi Experimental method. The three extensible vertical links and the three movable horizontal forcers provided the platform system with 6 degrees of freedom. The whole working space of the platform was determined by many control factors, of which the dominating ones were: the radius of the upper platform, R_P; the radius of the base platform, R_B; the height of the upper platform, Zh; and the leg length L. Therefore, our objective was to find values of the control factors such that the optimal working space could be obtained. Before implementing our design, the three movable synchronous linear motors had been purchased, so this constraint needed to be considered in our mechanism design.

5.1 Taguchi experimental method

A matrix experiment consists of a set of experiments in which the settings of the various parameters for study are changed from one experiment to another. Conducting matrix experiments using the orthogonal arrays allows the effects of several parameters to be determined efficiently; furthermore, it is an important technique for achieving robust design.

The optimal mechanism of the platform was designed to maximize the working space (translation and rotation) of the moving platform under constraint of the slide range of the translators of the linear motors and to extend the range of the AC motors. In this study, we used the pre-specified slide range 270*mm*, and the extensible length of the link was set to $l_i = 300mm$. In order to find the maximal working space, we needed to use the inverse kinematics algorithm to find the maximal position and orientation under the above constraints. To obtain the optimal mechanism design, we needed to find the optimal control factors such that the largest attitude change could be obtained. Firstly, we chose control factors, and we then set the levels of the control factors as shown in Table 1.

Table 1. Control factors and their levels in the first experiment.

Control Factor	Level		
	1	2	3
A. Upper Platform (R_p), mm	A1	A2	A3
B. Base Platform (R_B), mm	B1	B2	B3
C. Height (Zh), mm	C1	C2	C3
D. Length of Leg (L), mm	D1	D2	D3

All 9 experiments were conducted using the optimal mechanism design. Each experiment corresponded to a specific set of control factors used to construct a corresponding platform. In each experiment, we calculated the largest working space (translation or rotation) for only a single axis of the upper platform using inverse kinematics; that is, we increased the displacement of the upper platform's mass center or the attitude angle of the upper platform and computed the length and the position of the leg using inverse kinematics until the leg ran out of the extensible range or slid out of the slideway; then, the S/N could be evaluated. Finally, all 9 experiments were be repeated using different control factors.

The optimization problem can be solved by finding the optimal values of R_P, R_B, Zh, and L such that the signal-to-noise (S/N) ratio, η_i, of the working space is maximized through the following conducted matrix experiment:

$$\eta_i = 10 * log_{10}\left(\begin{array}{l} w_X * \dfrac{X^2}{X^2{}_{max}} + w_Y * \dfrac{Y^2}{Y^2{}_{max}} \\ + w_Z * \dfrac{Z^2}{Z^2{}_{max}} + w_\varphi * \dfrac{Roll^2}{Roll^2{}_{max}} \\ + w_\theta * \dfrac{Pitch^2}{Pitch^2{}_{max}} + w_\phi * \dfrac{Yaw^2}{Yaw^2{}_{max}} \end{array}\right) \quad (46)$$

$i = 1 \sim 9,$

where X, Y, Z, *Roll*, *Pitch*, and *Yaw* are the experimental values in the corresponding experiment. X_{max}, Y_{max}, Z_{max}, $Roll_{max}$, $Pitch_{max}$, and Yaw_{max} were the maximal values in all the experiments, and w_X, w_Y, w_Z, w_ϕ, w_q and, w_ψ were the weighting factors.

5.2 Simulation of the optimal mechanism design

To simulate this architecture, we set the initial values of levels 2 based on accumulated experience and the preliminary simulation results as shown in Table 3.

After the value of η_i for each experiment was computed, the next step was to estimate the effect of each control factor on the working space. The average η for each level of the four control factors could be obtained as shown in Table 4. For example,

Table 3. Control factors and their level in the first experiment.

Control Factor	Level		
	1	2	3
A. Upper Platform (R_p), mm	300	350	400
B. Base Platform (R_B), mm	1000	1050	1100
C. Height (Zh), mm	500	550	600
D. Length of Leg (L), mm	270	300	330

Table 4. Analysis of the optimal mechanical size.

Control Factor	Level(η)		
	1	2	3
A. R_P	8.031	7.239	6.650
B. R_B	7.168	7.598	7.155
C. Zh	7.198	7.413	7.309
D. L	6.919	7.394	7.608

$$\eta_{A1} = \frac{1}{3}(\eta_1 + \eta_2 + \eta_3) = 8.031.$$

In the first experiment, the working space of the yawing angle was found to be insufficient, so the weighting parameter related to the yawing contribution was decreased to enlarge the yawing working space in (46) and to enhance the importance of the yawing activity distinctively.

From the experimental results shown in Table 4, we can find the optimal condition $A_1B_2C_2D_3$: R_P = 300 mm, R_B = 1050 mm, Zh = 550 mm, L = 330 *mm*.

Substituting these values into the inverse kinematics equation, we can get the maximum working space:

$$X = \pm\begin{matrix}155\\155\end{matrix}\text{mm}, Y = \pm 135\text{mm}, Z = \pm\begin{matrix}153\\187\end{matrix}\text{mm},$$

$$Roll = \pm 64°, \text{Pitch} = \pm\begin{matrix}52°\\143°\end{matrix}, \text{Yaw} = \pm 51°.$$

Continue to do the matrix experiment, we can get the 3rd optimal experimental result , which is in the level condition $A_1B_2C_2D_3$, that is,

$$R_P = 230 \text{ mm}, R_B = 1050 \text{ mm},$$

$$\text{Zh} = 550 \text{ mm}, \text{L} = 400 \text{ mm}.$$

Based on the experimental results, we can analyze the effects of the control factors and estimate their trend for maximizing the working space as follows:

1. The experimental results demonstrated the trend of getting the optimal mechanism where the size of the upper platform becomes smaller and smaller, but the size of base platform becomes larger and larger.
2. Owing to failure to any mechanism hardware constraints in the experiment, the results results are rather ideal. Really, the practical mechanism must be constrained by some conditions, such as the constraint of the spherical joint and the physical constraints of all legs, it is impossible to get the ideal result of experiment as in the software simulation.

VI. CONCLUSION

The optimal mechanism design was obtainedand dynamic analysis of a 3-leg 6-DOF high performance platform system was performed in this study. A new architecture was implemented and a 3-leg 6-DOF platform system was built using the optimal mechanical size. This kind of architecture using the hybrid (linear and AC) motors yields high performance of motions, especially in terms of speed and working space. The novel result for the maximal working angles (more than 50°) is the significant contribution of this architecture. The Taguchi Experimental Method was applied to design the optimal mechanism of the platform system, and the results were used as actual data to build the platform system.

Using the superior working space of the special architecture and the high performance capability of the hybrid motors, we have developed a spatial disorientation training device. In this training device, we incorporate a 360° continuous yaw motion base into the platform system. This system can be used to simulate the most serious spatial illusion, and provides a simulation environment of spatial disorientation.

ACKNOWLEDGEMENT

This research was sponsored by National Science Council, Taiwan, R.O.C. under NSC grant 90-2212-E-035-021.

REFERENCES

1. Stewart, D., "A Platform with Six Degrees-of-freedom," *Proc. Inst. Mech. Eng*., Vol. 180, Part 1, No. 5, pp. 371-386 (1965).
2. Fichtert, E. F., "A Stewart Platform-based Manipulator: General Theory and Practical Construction," *Int. J. Rob. Res.*, Vol. 5, No. 2, pp. 157-182 (1986).
3. Ma, O. and J. Angeles, "Architecture Singularities of Parallel Manipulators," Vol. 7, pp. 23-27 (1992).
4. Ji, Z., "Workspace Analysis of Stewart Platform via Vertex Space," *J. Rob. Syst*., Vol. 13, pp. 631-639 (1994).
5. Liu, K. and F. Lewis, "The Singularity and Dynamics of a Stewart Platform Manipulator," *J. Int. Rob. Syst*., Vol. 8, pp. 287-308 (1993).
6. Hao, Z. and W. Qiyi, "The Kinematics and Workspace Analyses of a Parallel Manipulator for Manufacturing," *Proc. IEEE Int. Conf. Ind. Technol*., pp. 647-650 (1996).
7. Lee, M. K. and K. W. Park, "Kinematic and Dynamic Analysis of a Double Parallel Manipulator for Enlarging Workspace and Avoiding Singularities," *IEEE Trans. Rob. Autom*., Vol. 16, pp. 1024-1034 (1999).

8. Kim, N.I. and C.W. Lee, "High Speed Tracking Control of Stewart Platform Manipulator via Enhanced Sliding Mode Control," *Proc. IEEE Int. Conf. Rob. Autom.*, pp. 2716-2721 (1998).
9. Ceccarelli, M., "A New 3 D.O.F. Spatial Parallel Mechanism," *Mechanism Machine Theory*, Vol. 32, 895-902 (1997).
10. Phadke, M. S., *Quality Engineering Using Robust Design*, Prentice-Hall, Englewood Cliffs, New Jersey, (1989).
11. Hwang, C. H., "Mechanism Design and Dynamic Analysis of a High-Speed Linear Motor Actuating Platform System," Master Thesis, Institute of Aeronautics and Astronautics, Chung-Hua University, Hsinchu, Taiwan (2000).